Redox Biology 48 (2021) 102175

Contents lists available at ScienceDirect

Redox Biology

journal homepage: www.elsevier.com/locate/redox

Embryonal erythropoiesis and aging exploit ferroptosis

Hao Zheng [a], Li Jiang [a], Tsuyoshi Tsuduki [b], Marcus Conrad [c,d], Shinya Toyokuni [a,e,*]

[a] Department of Pathology and Biological Responses, Nagoya University Graduate School of Medicine, Nagoya, 466-8550, Japan
[b] Laboratory of Food and Biomolecular Science, Graduate School of Agriculture, Tohoku University, 468-1, Aoba, Aramaki, Aoba-ku, Sendai, 980-0845, Japan
[c] Helmholtz Zentrum München, Institute of Metabolism and Cell Death, 85764, Neuherberg, Germany
[d] Pirogov National Research Medical University, Laboratory of Experimental Oncology, Ostrovityanova 1, Moscow, 117997, Russia
[e] Center for Low-temperature Plasma Sciences, Nagoya University, Furo-cho, Chikusa, Nagoya, 464-8603, Japan

ARTICLE INFO

Keywords:
Ferroptosis
Iron
4-Hydroxy-2-nonenal
Erythropoiesis
Aging

ABSTRACT

Ferroptosis is a form of regulated cell necrosis, as a consequence of Fe(II)-dependent lipid peroxidation. Although ferroptosis has been linked to cancer cell death, neurodegeneration and reperfusion injury, physiological roles of ferroptosis have not been elucidated to date mostly due to the lack of appropriate methodologies. Here, we show that 4-hydroxy-2-nonenal (HNE)-modified proteins detected by a HNEJ-1 mouse monoclonal antibody is a robust immunohistochemical technology to locate ferroptosis in tissues in combination with morphological nuclear information, based on various models of ferroptosis, including erastin-induced cysteine-deprivation, conditional *Gpx4* knockout and Fe(II)-dependent renal tubular injury, as well as other types of regulated cell death. Specificity of HNEJ-1 with ferroptosis was endorsed by non-selective identification of HNE-modified proteins in an Fe (II)-dependent renal tubular injury model. We further comprehensively searched for signs of ferroptosis in different developmental stages of *Fischer-344* rats from E9.5–2.5 years of age. We observed that there was a significant age-dependent increase in ferroptosis in the kidney, spleen, liver, ovary, uterus, cerebellum and bone marrow, which was accompanied by iron accumulation. Not only phagocytic cells but also parenchymal cells were affected. Epidermal ferroptosis in ageing *SAMP8* mice was significantly promoted by high-fat or carbohydrate-restricted diets. During embryogenesis of *Fischer-344* rats, we found ferroptosis in nucleated erythrocytes at E13.5, which disappeared in enucleated erythrocytes at E18.5. Administration of a ferroptosis inhibitor, liproxstatin-1, significantly delayed erythrocyte enucleation. Therefore, our results demonstrate for the first time the involvement of ferroptosis in physiological processes, such as embryonic erythropoiesis and aging, suggesting the evolutionally acquired mechanism and the inevitable side effects, respectively.

1. Introduction

Ferroptosis is a type of regulated cell necrosis as a consequence of iron-dependent lipid peroxidation, which was first reported on *H-ras* mutated fibrosarcoma cells after cysteine depletion with erastin [1,2]. Current interpretation of the phenomenon is the predominance of catalytic Fe(II) over antioxidant sulfhydryls inside the cell as a switch toward ferroptosis [3]. This newly defined cell death attracted the interests of researches of various areas, leading to the revised understanding of pathologies, not only in cancer [4] but also in neurodegenerative diseases [5] and reperfusion injury [6].

Ferroptosis inhibitors are reportedly protective in preclinical models of neurodegenerative diseases, including Parkinson's, Huntington's and Alzheimer's disease [7–10]. Carcinogenesis is now recognized as a process to obtain ferroptosis-resistance by acquisition of somatic mutations [4,11,12]. Of note, many drug-resistant and aggressive cancer cells may depend on the suppression of ferroptosis for growth and survival [13], which may represent a therapeutic vulnerability for such cancers [12,14,15]. Ferroptosis is also associated with intestinal ischemia-reperfusion injury, where ACSL4 activation plays a critical role in this lethal process [16]. Overexpression of a few molecules has been considered as a biomarker of ferroptosis. For example, ACSL4 is considered as a potential biomarker and driver of ferroptosis for its role in enhancing the polyunsaturated fatty acid content in phospholipids [17,18]. *Prostaglandin-endoperoxide synthase 2 (PTGS2)*, a gene encoding cyclooxygenase-2 (COX-2), has been described to be increased in cells treated with ferroptosis inducers [19]. However, up until now a

* Corresponding author. Department of Pathology and Biological Responses, Nagoya University Graduate School of Medicine, 65 Tsurumai-cho, Showa-ku, Nagoya, Japan.
E-mail address: toyokuni@med.nagoya-u.ac.jp (S. Toyokuni).

https://doi.org/10.1016/j.redox.2021.102175
Received 15 October 2021; Accepted 28 October 2021
Available online 30 October 2021

Abbreviations

ACSL4	acyl-coenzyme A synthetase long-chain family member 4
ALDHs	aldehyde dehydrogenases
BSA	bovine serum albumin
CHR diet	carbohydrate restricted diet
cKO	conditional knockout
COX-2	cyclooxygenase-2
Fe-NTA	ferric nitrilotriacetate
Fer-1	ferrostatin-1
FFPE	formalin-fixed paraffin-embedded
GAPDH	glyceraldehyde 3-phosphate dehydrogenase
GPX4	glutathione peroxidase 4
HF diet	high fat diet
HNE	4-hydroxy-2-nonenal
IP	immunoprecipitation
KLH	keyhole limpet hemocyanin
Lipro-1	liproxstatin-1
15-LOX	15-lipoxygenase
MEFs	mouse embryonic fibroblasts
MS	mass spectrometry
NB	newborn
8-OHdG	8-hydroxy-2′-deoxyguanosine
PFA	paraformaldehyde
PLP	prolactin-like protein
PSM	peptide spectrum matches
PTGS2	prostaglandin-endoperoxide synthase 2
RBC	red blood cells
ROS	reactive oxygen species
RT	room temperature
SAMP8	senescence-accelerated prone mice 8
STS	staurosporine
TCA	tricarboxylic acid
TfR1	transferrin receptor 1
TGCs	trophoblast giant cells

physiological meaning of ferroptosis has not been established likely due to the lack of easy-to-perform and reliable methodologies and tools to directly monitor ferroptosis in physiological and pathophysiological contexts.

Here, we set out to search for a proper strategy to discover "physiological ferroptosis". Pathological analyses of the experimental rodents provide with optimal screening for ferroptosis if an appropriate antibody is designed for the detection of ferroptosis initiated by different mechanisms. An iron chelate, ferric nitrilotriacetate (Fe-NTA), induced ferroptosis via Fenton reaction specifically in the renal proximal tubules when injected intraperitoneally, leading to a high incidence of renal cell carcinoma in rodents after repeated injections [20–23]. Indeed, excess iron has been associated with carcinogenesis [11,24]. We previously found that 4-hydroxy-2-nonenal (HNE) is the most sensitive marker among lipid peroxidation products, using Fe-NTA-induced oxidative renal tubular ferroptosis model [25,26]. Based on the results, we developed five different monoclonal antibodies against hemiacetal structure of Michael adducts in HNE-modified proteins [27,28]. We started from reevaluating those antibodies and found that HNEJ-1 presents the most promising candidate for monitoring ferroptotic events in tissues and protein isolates.

2. Materials and methods

2.1. Cell line and media

Human fibrosarcoma cell line HT1080 was purchased from JCRB (Japan). HT1080 cells was cultured in EMEM (051–07615, Wako, Osaka, Japan), containing 10% fetal bovine serum (Biowest; Nuaillé, France) and 1% Antibiotic–Antimycotic (15240-062; Invitrogen) under 5% CO_2 atmosphere.

2.2. Materials

Erastin (Cat. #571203-78-6) was purchased from Cayman Chemical (Ann Arbor, MI). Ferrostatin-1 (Fer-1; Cat. #SML0583), (1S,3R)-RSL3 (Cat. #SML2234) liproxstain-1 (Lipro-1; Cat. # SML1414) and deferoxamine mesylate salt (DFO, Cat. #D9533) were from Sigma-Aldrich (St. Louis, MO). Staurosporine (Cat. #9953) was from Cell Signaling (Danvers, MA). Other chemicals used were of analytical grade.

2.3. Antibodies

MAbs HNEJ-1∼5 were produced, purified and analyzed as previously described [27,28].

2.4. Cell viability

In these studies, 5,000 HT1080 cells/well were seeded in 96-well plates (Cat. #167008, Thermo Fisher Scientific; Waltham, MA) and incubated for 12 h/37 °C. After the indicated treatment, medium was replaced with fresh serum-free EMEM containing WST-8 reagent (the cell count reagent SF, Cat. #07553, Nacalai Tesque, Kyoto, Japan) and incubated for 1 h at 37 °C. Plates were scanned at 450 nm with a Multiscan FC plate reader (Thermo Fisher Scientific).

2.5. Cell block preparation

After the indicated treatment, cells were harvested and centrifuged at 300×*g* for 3 min and the supernatant was replaced with 4% (w/v) paraformaldehyde (PFA, Cat. #43368 Alfa Aesar™). Next, the cells were embedded in paraffin to be handled as a routine tissue block. The cell block sections were stained with hematoxylin & eosin (HE) or prepared for immunohistochemistry.

2.6. Intracellular localization of HNE

HT1080 cells (1.5×10^5) were cultured on 35-mm glass bottom dishes (D11131H and D11140H, Matsunami; Kishiwada, Japan) for 12 h at 37 °C. For the detection of HNE modification in organelles, cells treated as indicated were stained with MitoTracker™ Deep Red FM (Cat. #M22426, Invitrogen; 60 nM) and LysoTracker™ Red DND-99 (Cat. #L7528, Invitrogen; 160 nM) in FluoroBrite DMEM (A1896702, Gibco, Thermo Fisher Scientific) for 30 min. Cells were then washed and fixed with 4% PFA for 10 min at room temperature (RT), followed by incubation with 0.1% (v/v) Triton X-100 for 5 min at RT. Blocking was performed with 3% (w/v) bovine serum albumin (BSA). The cells were then incubated with the primary antibody HNEJ-1 (5 μg/ml) in 1% BSA at RT, washed 3 times with PBS and then incubated with the secondary antibody, goat anti-mouse IgG (1:2000) conjugated with Alexa Fluor 488 (Invitrogen) for 1 h at RT. For the detection of HNE modification on plasma membrane, cells treated as indicated were washed and fixed with 4% (w/v) PFA for 10 min at room temperature (RT). Blocking was performed with 3% (w/v) BSA. The cells were then incubated with the primary antibody HNEJ-1 (5 μg/ml) in 1% BSA at RT, washed 3 times with PBS and then incubated with the secondary antibody, goat anti-mouse IgG (1:2000) conjugated with Alexa Fluor 488 (Invitrogen) for 1 h at RT. *Z*-stack (at least 10 sections) with a section depth of 0.23 μm

were acquired by LSM880 (Carl Zeiss, Oberkochen, Germany). Colocalization coefficients were measured with ZEN 3. 3 software, using the average value from 8-10 sections per cell for Mitotracker and 3-5 sections per cell for Lysotracker.

2.7. Immunofluorescence

HT1080 cells (1.5×10^5) were cultured on 35-mm glass bottom dishes (Matsunami) for 12 h at 37 °C. After the indicated treatment, cells were then fixed with 4% (w/v) PFA for 10 min/RT, washed 3 times using PBS, incubated with 0.1% (v/v) Triton X-100 and blocked for 1 h at RT with 3% (w/v) BSA. The cells were then incubated overnight at 4 °C with a primary antibody, either HNEJ-1 (5 μg/ml), anti-ACSL4 (Cat. # PA5-27137, 1:1000, Invitrogen) or anti-cleaved caspase-3 (Cat. #5A1E; 1:500 dilution; Cell signaling), washed 3 times with PBS and incubated with a secondary antibody, either Alexa Fluor® Plus 488 or Alexa Fluor® Plus 568 (Invitrogen). LSM880 was used to analyze intensity and localization. More than fifty cells were quantified with ZEN 3.3 software for integration of each fluorescence (wavelength) area via excluding the cellular background. The relative intensity per cell in arbitrary units is shown.

2.8. Acute renal damage model

For the study of acute renal damage, a single intraperitoneal injection of ferric nitrilotriacetate (Fe-NTA; 15 mg iron/kg) was carried out using 6-week-old male Wistar rats (Japan SLC, Hamamatsu, Japan) [25]. Three hours after Fe-NTA administration, the rats were euthanized. Both of the kidneys were immediately excised and stored frozen at −80 °C until use. A small portion of the kidney was fixed with 10% neutral buffered formalin overnight for histological examination with HE staining or immunohistochemistry of paraffin-embedded specimens. All the procedures were performed in accordance with the national guidelines and approved by the animal experiment committee of Nagoya University Graduate School of Medicine.

2.9. Kidney of Gpx4 conditional knockout (cKO) mice

Kidney sections from *Gpx4* cKO mice were prepared as described [29]. Kidneys from *wild-type C57*BL*/6* mice (Japan SLC, Hamamatsu, Japan) served as a control.

2.10. Animals for physiological development study

For the study of physiological development, *Fischer-344* rats (Japan SLC) of different ages (E9.5, E13.5, E15.5, E18.5, new born [day 6], weaning age [3–4 wk], young adults [8 wk], adults [3.5 and 6 months] and the aged [2.5 y]) were euthanized. All the organs were harvested and fixed with 10% neutral buffered formalin overnight for histological examination with HE staining, Berlin blue staining or immunohistochemistry of paraffin-embedded specimens. Two ferroptosis inhibitors (Lipro-1 and Fer-1) were used to demonstrate the involvement of ferroptosis in embryonic erythropoiesis. For the administration of Lipro-1, pregnant rats (day 13) were intraperitoneally injected with 10 mg/kg Lipro-1 consecutively for 4 days. Regarding the administration of Fer-1, pregnant rats (day 13) were intravenously injected with 0.8 mg/kg Fer-1 at day 13 and day 15. Control groups were administrated with Ringer's lactate solution (Cat. #14500AMZ02080; Otsuka Pharmaceutical Co., Ltd, Tokyo, Japan) in the same manner as ferroptosis inhibitor groups. At day 18.5, embryos were harvested and fixed for HE staining or for blood collection. All the procedures were performed in accordance with the national guidelines and approved by the animal experiment committee of Nagoya University Graduate School of Medicine.

2.11. Skin senescence model and diets

Skin sections were prepared as described [30]. Briefly, three-weeks-old male *SAMP8* mice (Japan SLC) were randomly divided into three groups: control (CO) group, fed a normal diet (Rodent diet, AIN-93G); HF group, fed a high-fat diet (part of cornstarch in AIN-93G was replaced with lard and cholesterol); and CHR group, fed a carbohydrate-restricted diet (low carbohydrate-high protein diet, in which milk casein replaced corn starch in the high-fat diet). At 49 weeks of age, the progression of the appearance of senescence was assessed. At 50 weeks of age, after a 12-h fasting, the mice were euthanized and the skin was removed. To examine ferroptosis in the epidermis, mouse skin was fixed in 10% formalin and embedded in paraffin. Vertical sections (5 mm) were cut, mounted on a glass slide for Masson's trichrome staining and immunohistochemistry.

2.12. Immunohistochemistry

Serial sections were prepared to enable better comparison of each immunostaining. Immunohistochemical staining was performed on 3 μm-thick paraffin-embedded sections after 10% neutral buffered formalin (FFPE). Briefly, after deparaffinization, the specimens were incubated with 0.3% H_2O_2 in methanol for the inhibition of endogenous peroxidase. Then, normal rabbit serum (diluted 1:75; Dako) for inhibition of non-specific binding of the secondary antibody, mAbs against HNE-modified proteins (HNEJ-1～5, Anti-8-OHdG mouse monoclonal antibody N45.1 [31]), biotin-labeled rabbit anti-mouse IgG serum (diluted 1:300; Dako) and avidin-biotin complex (diluted 1:100; Vector Laboratories, Burlingame, CA) were sequentially used. 3,3-Diaminobenzidine solution (Dako Liquid DAB, K3466) was used for visualizing the antibody complexes. Procedures using nonimmune mouse IgG1 instead of HNEJ-1～5 antibody showed no positivity. For some experiments, immunohistochemical staining using anti-cleaved caspase-3, anti-ACSL4, anti-PTGS2 (Cat. #ab15191, Abcam) or HNEJ-1 antibody was performed with a standard polymer detection system according to the instructions of the manufacturer using Bond-MAX automated IHC Instruments (Leica). Tissues were counterstained with hematoxylin, dehydrated and mounted. Deposition of lipofuscin (yellow-brown pigment granules) in organs lead to disturbance on the visualization of positivity when using DAB as a peroxidase substrate. Thus, HistoGreen was used as a substrate instead of DAB for the immunohistochemistry of organs in different developmental stages. Briefly, after deparaffinization, the specimens were incubated with 3% H_2O_2 in methanol for the inhibition of endogenous peroxidase. Either HNEJ-1 (5 μg/ml), anti-CD68 (Cat. #MCA341 1:500 dilution, Bio-rad), anti-ACSL4 (1:500 dilution) or anti-PTGS2 (1:500 dilution) antibody, and Histofine® Simple Stain MAX PO (MULTI) (Nichirei Biosciences INC) were sequentially applied. HISTOPRIME (Cat. #E109; Cosmo Bio, Tokyo, Japan) was used for color development. Tissues were counterstained with hematoxylin, dehydrated and mounted. Relative quantification of the staining was performed as previously described [31], using randomly selected 3–6 photo files, each of which contained >100 cells.

2.13. Immunoprecipitation

A single intraperitoneal injection of Fe-NTA (15 mg iron/kg) was carried out as previously described, using 6-week-old specific pathogen-free male Wistar rats. The rats were euthanized 3 h after Fe-NTA administration. The damaged kidneys and normal kidneys were immediately collected and lysed to extract proteins. Lysate (lysis buffer; 20 mM Tris-HCl, PH 7.4, 0.1% NP40, proteinase inhibitor) of 400 μg were incubated with 10 μL HNEJ-1 at 4 °C for 3 h, and then with Protein G Sepharose® 4 Fast Flow (GE17-0618-01, Sigma Aldrich) for 1 h at 4 °C. The precipitates were washed three times with HEPES buffer and then denatured by heating in sample buffer for 5 min at 95 °C. The immunoprecipitates were resolved on 10% SDS-PAGE, and the proteins were

transferred to Hybond-Ptm membranes. Immunoblotting was performed using antibodies against GAPDH (Cat. #A10868; 1/1000 dilution; ABclonal) and GPX4 (Cat. #ab125066; 1/1000 dilution; Abcam).

2.14. Mass spectrometry

Acute renal damage model was used to identify HNEJ-1-targeted proteins. Briefly, a single intraperitoneal injection of Fe-NTA (15 mg iron/kg) was carried out as described, using 6-week-old specific pathogen-free male Wistar rats. Three h after Fe-NTA administration, the rats were euthanized and kidneys were harvested immediately. Kidneys (control and after Fe-NTA injection) were homogenized in lysis buffer, and tissue lysate samples were collected after centrifuge (15, 000×g, 4 °C). Tissue lysate sample of 400 μg each (control and after Fe-NTA injection) were incubated with 10 μl HNEJ-1 antibody for 3 h at 4 °C. Protein G Sepharose beads (GE17-0618-01, Sigma Aldrich) were added to each tissue lysate sample and were washed three times by 0.1 M HEPES buffer after 1-h incubation. For in-solution digestion, the proteins were detached from the bead pellets by degeneration with 6 M guanidinium chloride and digested by trypsin for 16 h at 37 °C after reduction and alkylation. The peptides were analyzed by LC-MS using an Orbitrap Fusion mass spectrometer (Thermo Fisher Scientific) coupled to an UltiMate3000 RSLCnano LC system (Dionex Co., Amsterdam, The Netherlands) using a nano HPLC capillary column (150 mm × 75 μm i.d.; Nikkyo Technos Co., Tokyo, Japan) via a nano electrospray ion source. The raw data was processed using either Proteome Discoverer 1.4 (Thermo Fisher Scientific) in conjunction with MASCOT search engine, version 2. 6.0 (Matrix Science Inc., Boston, MA) for protein identification. Enriched HNE-modified proteins were ranked as folds of the number of peptide spectrum matches (PSM) between the control and the kidney after Fe-NTA injection.

2.15. Protein extraction and immunoblotting

Whole blood from embryos were collected and lysed to extract proteins. The primary antibodies used for immunoblotting were against Lamin B (Cat. #sc-6217; 1:1000 dilution; Santa Cruz Biotechnology) and TfR1 (Cat. #13–6800; 1:1000 dilution, Invitrogen). Antibodies against β-actin (Cat. #clone AC-15; 1/5000 dilution; Sigma) was used as protein-loading controls.

2.16. Statistics

All statistical analyses were performed with GraphPad Prism 5 software (GraphPad Software, La Jolla, CA). Significance of difference was determined by unpaired *t*-test, one-way ANOVA or two-way ANOVA, followed by *Tukey's* multiple comparison test. Significance was defined as $P < 0.05$.

3. Results

3.1. HNEJ-1 is useful for detecting ferroptosis by immunohistochemistry

We previously produced five distinct monoclonal antibodies, called HNEJ-1∼5, against HNE-modified keyhole limpet hemocyanin (KLH) and characterized which Michael adducts among His, Lys and Cys adducts each recognizes [27,28]. HT-1080 fibrosarcoma cells treated with erastin (a ferroptosis inducer) with or without ferrostatin-1 (Fer-1, a ferroptosis inhibitor) were used as a ferroptosis model (Fig. S1A) to check the sensitivity and specificity and suitability of these five monoclonal antibodies for immunohistochemistry. Immunostaining of two potential ferroptosis markers, PTGS2 and ACSL4, were also evaluated to confirm this classic ferroptosis model (Fig. S1C). Among the five antibodies, HNEJ-1 showed both high sensitivity and specificity in erastin-treated cells in comparison to non-treated control cells in cell-block sections. HNEJ-2 showed high positivity in both ferroptotic and control cells and indicated high sensitivity but relatively low specificity, suggesting a requirement to find an appropriate window for a variety of tissue and pathology conditions. HNEJ-3∼5 showed low sensitivity in this ferroptosis model (Fig. 1A). Furthermore, the sensitivity of HNEJ-1 was also tested by immunofluorescence in ferroptosis models triggered by two distinct inducers (erastin and RSL3) in the presence or absence of Fer-1 or deferoxamine mesylate (DFO; an iron chelator). HNEJ-1 again exhibited specific immunostaining in ferroptotic cells, as confirmed by ACSL4 immunostaining (Fig. 1BC, Fig. S1B). Thus, HNEJ-1 is useful for detecting ferroptosis by immunohistochemistry.

3.2. Specificity of HNEJ-1 on cell death mode

To test the specificity of HNEJ-1 on different cell death modes, we used staurosporine (STS)-induced apoptosis and H_2O_2-induced acute necrosis model after adjusting the experimental condition (Fig. S1DE). HNEJ-1 immunostaining did not increase during apoptosis in comparison to cleaved caspase-3 immunostaining (Fig. 2A). Furthermore, immunohistochemistry of block sections of STS-induced apoptotic cells revealed similar results, indicating that HNEJ-1 can distinguish ferroptosis from apoptosis (Fig. 2B). The expression of ACSL4 was not increased in STS-induced apoptotic cells, whereas a slight increase in PTGS2 was observed in these cells (Fig. 2B). Although PTGS2 has been widely demonstrated as an inhibitory factor of apoptosis [32], protective effect exerted by COX-2-derived prostanoids by decreasing apoptosis was reported in liver fibrosis [33]. Furthermore, STS was reported to induce PTGS2 expression in rat peritoneal macrophages without referring to apoptosis [34]. Whether the observation of increased PTGS2 in STS-treated cells is related to the induction of apoptosis needs further investigation. We then incubated HT1080 cells with H_2O_2 to assess whether HNEJ-1 can detect H_2O_2-induced cell death, which is an oxidative stress-induced necrosis associated with Fenton reaction. DFO but not ferrostatin-1 reversed H_2O_2-induced cell death to some extent, suggesting that this cell death is partially iron-dependent (Fig. S1E). We observed moderately increased positivity of HNEJ-1 in cell-blocks of necrotic cells with the increased expression of ACSL4 in comparison to control cells (Fig. 2C). These results indicate that ferroptosis was partially involved in H_2O_2-induced cell death although elevated PTGS2 expression was not observed in these cells.

3.3. Subcellular localization of HNE-modified proteins recognized by HNEJ-1 in cell models

We co-stained HNEJ-1 with Mitotracker and Lysotracker in HT1080 cell models of ferroptosis triggered by erastin [2]. When ferroptosis was induced, colocalization coefficients and weighted colocalization coefficients were increased both for HNEJ-1 and Mitotracker, indicating an increased immunostaining of HNEJ-1 in mitochondria (Fig. 3A). Although elevated colocalization coefficients/weighted colocalization coefficients were increased for Lysotracker in ferroptotic cells, no increment in coefficients was observed for HNEJ-1 and the coefficients were extremely low (Fig. S2), suggesting that HNE modification in lysosomes accounts for the minimal part of total HNE-modified proteins. Unexpectedly, the immunostaining was localized in the other cytoplasmic compartments as well. Thus, we decided to identify the HNE-modified proteins later and further immunostained the cells without permeabilization by HNEJ-1. We detected an increase in plasma membrane immunopositivity of ferroptotic cells, triggered either by erastin or RSL3 (Fig. 3B).

3.4. Detection of ferroptosis with HNEJ-1 in animal models

We thereafter evaluated HNEJ-1 for the detection of ferroptosis in *in vivo* pathologic situations and in different species. We first applied HNEJ-1 with immunohistochemistry to the kidney of *Gpx4* cKO mouse,

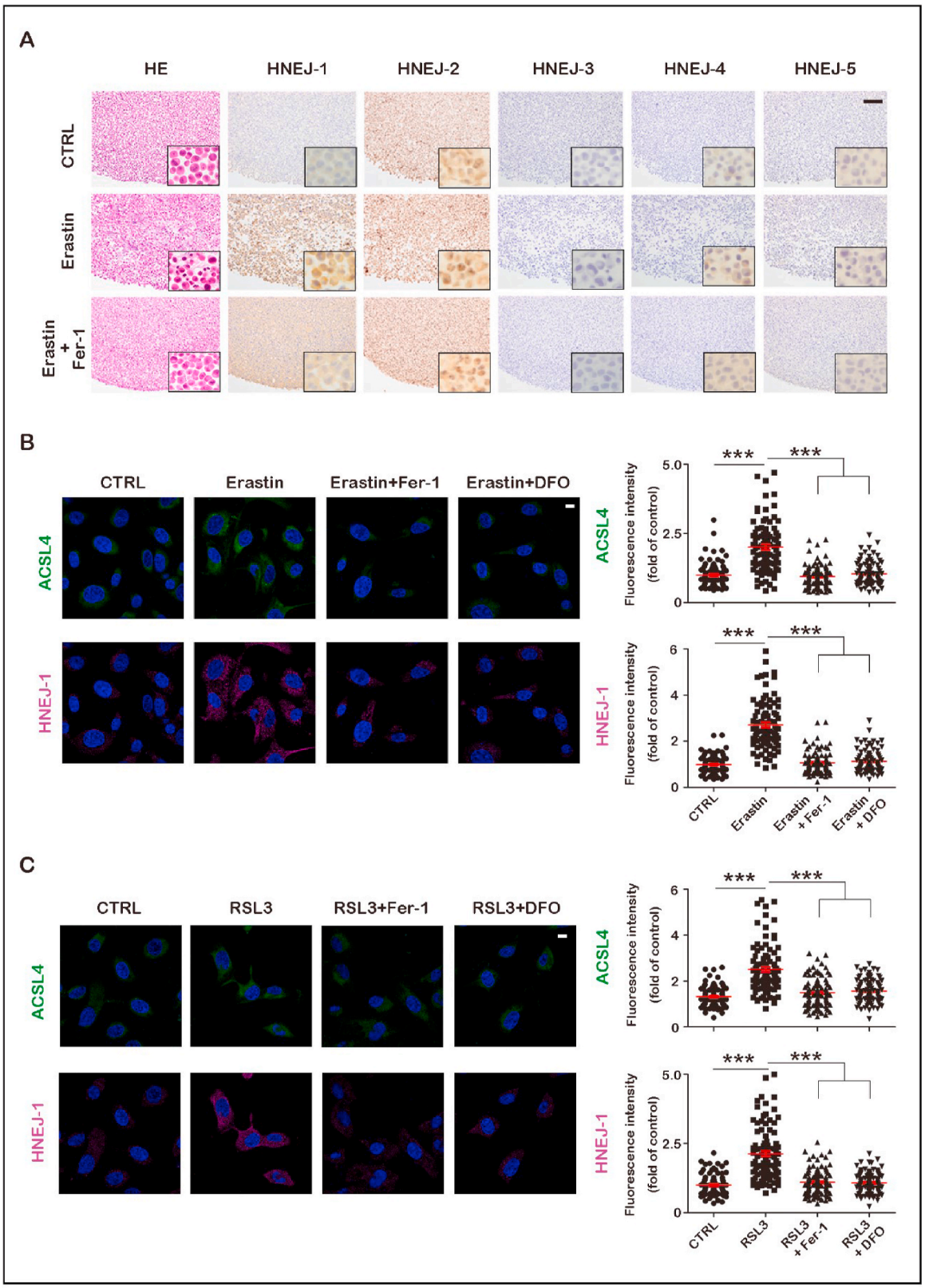

Fig. 1. *Identification of HNEJ-1 as a ferroptosis-specific antibody among five monoclonal anti-HNE antibodies.* **(A)** Human fibrosarcoma HT1080 cells were treated with erastin (10 μM) in the presence or absence of ferrostatin-1 (Fer-1, 5 μM) for 12 h. Then, they were harvested and fixed with 4% paraformaldehyde (PFA) for cell block. Immunohistochemistry was performed with HNEJ-1∼5, respectively (scale bar = 100 μm). **(B)** Human fibrosarcoma HT1080 cells were treated with erastin (10 μM) in the presence or absence of Fer-1 (5 μM) or deferoxamine mesylate (DFO, 500 μM) for 12 h. Then, they were fixed with 4% PFA. After blocking, cells were incubated with HNEJ-1 or anti-ACSL4 and finally observed with confocal microscopy (scale bar = 10 μm). **(C)** Human fibrosarcoma HT1080 cells were treated with RSL3 (0.25 μM) in the presence or absence of Fer-1 (5 μM) or DFO (500 μM) for 3 h. Then, they were fixed with 4% PFA. After blocking, cells were then incubated with HNEJ-1 or anti-ACSL4 antibody and finally observed with confocal microscopy (scale bar = 10 μm). Representative data are shown based on 3 independent experiments and the analysis is shown as means ± SEM (n = 3); ***P < 0.001 *vs* control (CTRL) unless indicated by bar. Refer to text for details.

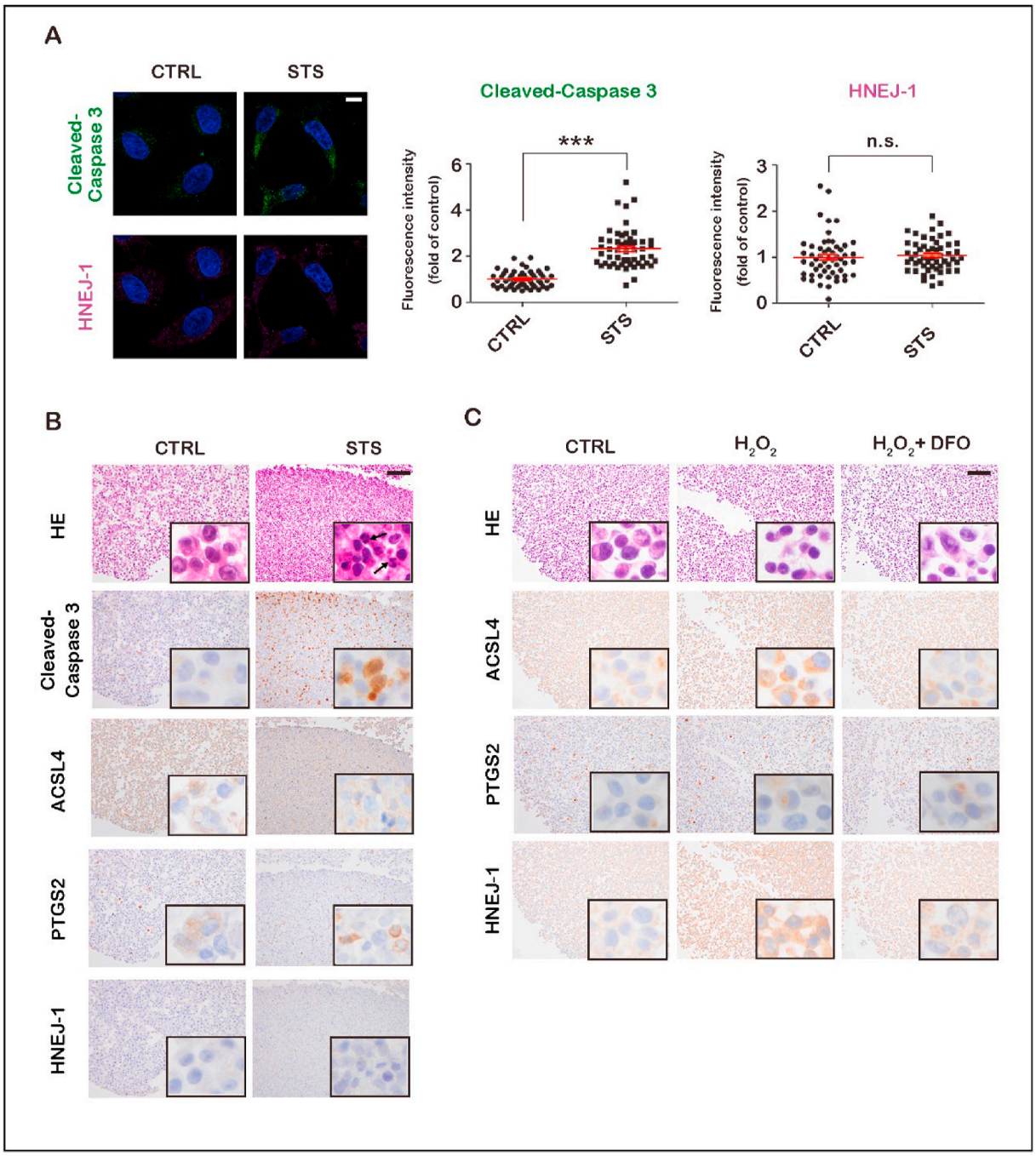

Fig. 2. *Specificity of HNEJ-1 as a ferroptosis marker using various cell death inducers.* (A) Human fibrosarcoma HT1080 cells were treated with staurosporine (STS, 1 μM) for 6 h. Then, they were fixed with 4% PFA. After blocking, cells were then incubated with HNEJ-1 or anti-cleaved caspase 3, and finally observed with confocal microscopy (scale bar = 10 μm). **(B)** Human fibrosarcoma HT1080 cells were treated with STS (1 μM) for 6 h. Afterwards, they were fixed with 4% PFA. Immunohistochemistry was performed with HNEJ-1, anti-cleaved caspase 3, anti-ACSL4 or anti-PTGS2 antibody (scale bar = 100 μm). **(C)** HT1080 cells were treated with hydrogen peroxide (500 μM) in the presence or absence of Fer-1 (10 μM) or DFO (500 μM) for 3 h. Subsequently, they were fixed with 4% PFA. Immunohistochemistry was performed with HNEJ-1, anti-ACSL4 or anti-PTGS2 antibody (scale bar = 100 μm). Representative data are shown based on 3 independent experiments and the analysis is shown as means ± SEM (n = 3); ***P < 0.001 *vs* CTRL unless indicated by bar. Refer to text for details.

where ferroptosis is prevalent [29]. HNEJ-1 showed significantly higher positivity in *Gpx4* cKO kidney in comparison to that of *wild-type* (Fig. 4A), confirming the usefulness of HNEJ-1. We next applied HNEJ-1 to iron-catalyzed Fenton reaction-based acute renal ferroptosis model by Fe-NTA in rats [23], which revealed intense immunopositivity in the renal proximal tubules in comparison to the control kidney (Fig. 4B). We observed increased expression of both ACSL4 and PTGS2 in these two renal ferroptosis models (Fig. 4A and B). Our results indicate that HNEJ-1 is useful to detect ferroptosis by immunohistochemistry.

3.5. Potential target proteins of HNEJ-1

We comprehensively identified HNE-modified proteins recognized by HNEJ-1, using the Fe-NTA-induced renal ferroptosis model as described above. Among the top 150 HNE-modified proteins, the distribution of subcellular localization was cytosol (30%), mitochondria (26.7%), secreted (26%), nuclear (23.3%), membrane (15.3%) and cytoskeleton (14%) (Table S1). We then summarized the top-20 enriched HNE-modified proteins based on their subcellular

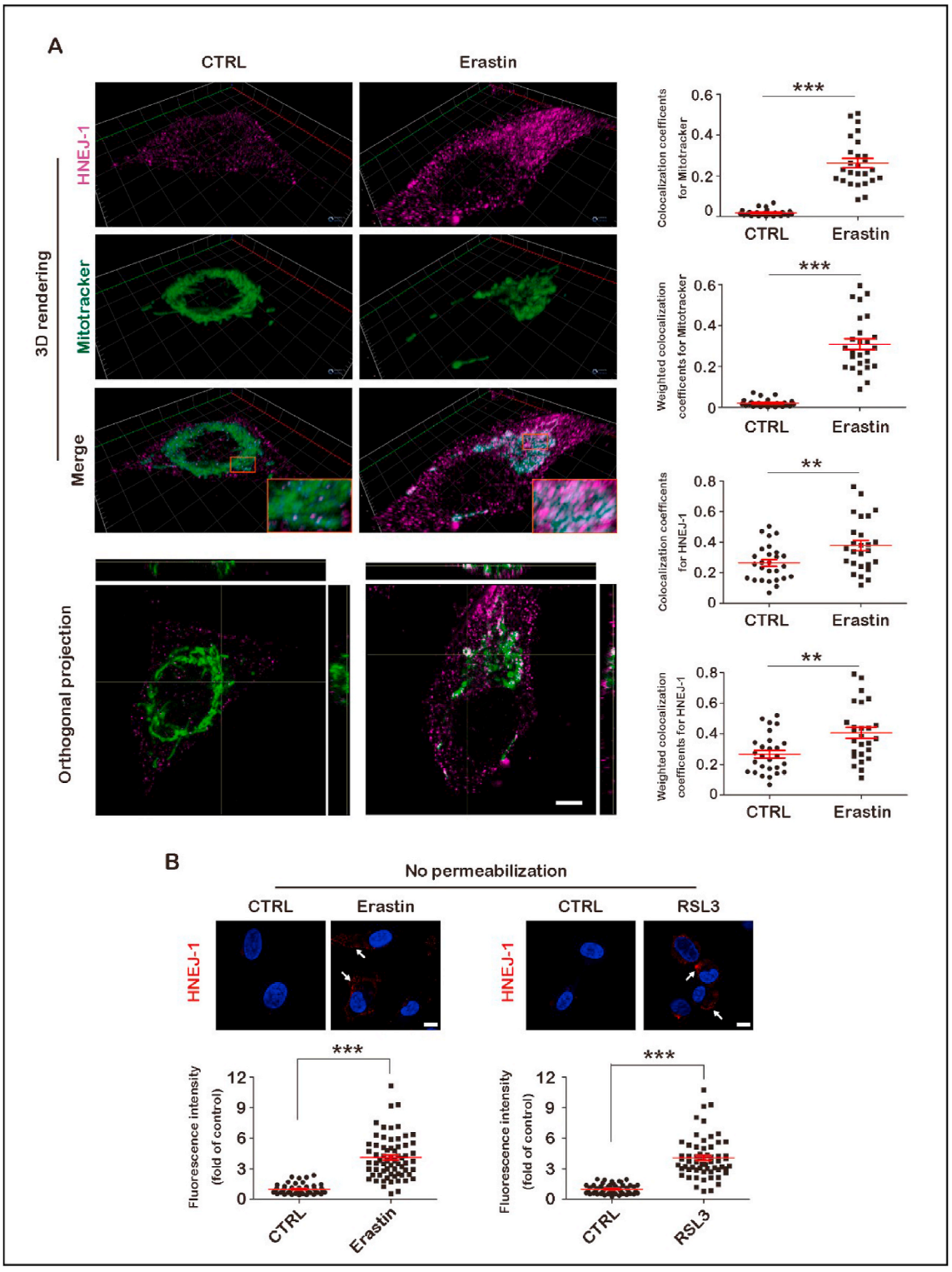

Fig. 3. *Intracellular targets of HNEJ-1 in ferroptotic cells.* (A) Human fibrosarcoma HT1080 cells were treated with erastin (10 μM) for 12 h. Cells were then stained for 30 min/37 °C with MitoTracker™ Deep Red FM. They were then fixed with 4% PFA. After blocking, cells were then incubated with HNEJ-1 for 1 h at room temperature and finally observed with confocal microscopy (1 unit for each axis = 5 μm for 3D rendering; scale bar = 5 μm for orthogonal projection). **(B)** Human fibrosarcoma HT1080 cells were treated with RSL3 (0.25 μM) for 3 h; or erastin (10 μM) for 12 h. Cells were then washed and fixed with 4% PFA. For the detection of HNE modification on the plasma membrane, cells were treated without permeabilization. After blocking, cells were incubated with HNEJ-1 antibody for 1 h at room temperature and finally observed with confocal microscopy (scale bar = 10 μm). Representative data are shown from 3 experiments and the analysis is shown as means ± SEM (n = 3); ***P < 0.001 *vs* CTRL unless indicated by bar. Refer to text for details. (For interpretation of the references to color in this figure legend, the reader is referred to the Web version of this article.)

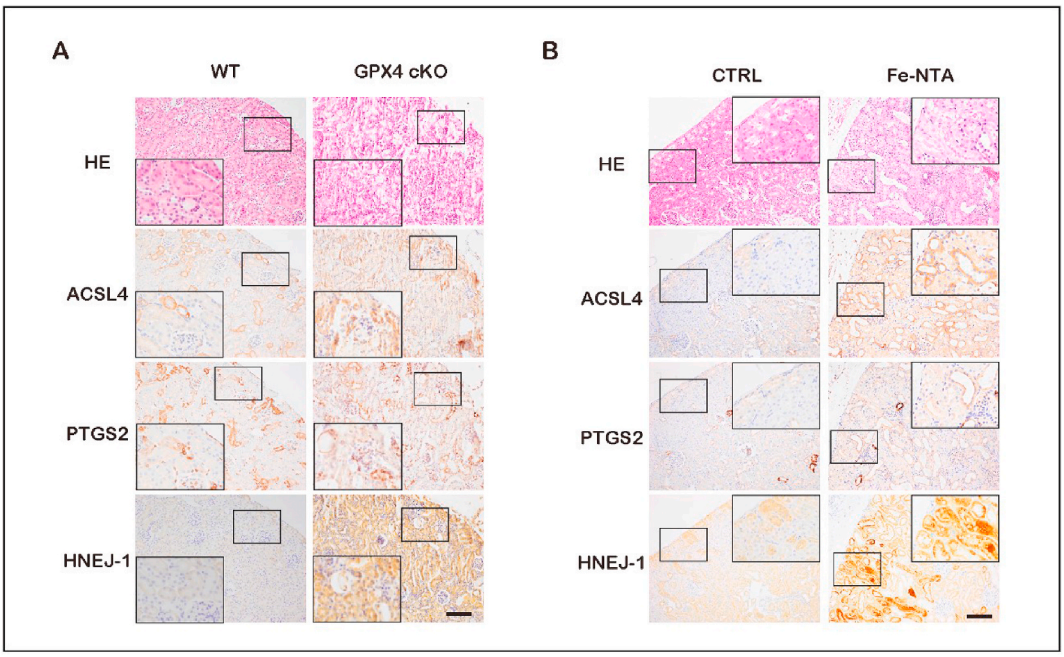

Fig. 4. *HNEJ-1 as a ferroptosis marker for immunohistochemistry in tissue.* **(A)** Immunohistochemical positivity on *Gpx4* conditional knockout kidney in comparison to *wild-type* kidney of *C57*BL*/6* mouse was evaluated with HNEJ-1, anti-ACSL4 or anti-PTGS2 antibody (scale bar = 100 μm). Representative data are shown based on 3 independent experiments. **(B)** Rats (*Wistar* strain, male, 6 weeks of age) were euthanized 3 h after administration of 15 mg iron/kg of Fe-NTA and a portion of the kidney was fixed with 10% neutral buffered formalin for immunohistochemistry. Immunopositivity in the renal proximal tubules 3 h after Fe-NTA administration was assessed with immunohistochemistry using HNEJ-1, anti-ACSL4 and anti-PTGS2 antibody (scale bar = 100 μm).

localization **(**Table S1**)**.

Glyceraldehyde 3-phosphate dehydrogenase (GAPDH) is a known target of HNE modification [35], identified in the present experiment **(**Table S1**)**. We performed immunoprecipitation followed by immunoblot analysis to confirm that GAPDH is indeed modified with HNE (Fig. S3A). The key regulator of ferroptosis, GPX4, was not the target of HNEJ-1 at this time point of ferroptosis but was already lost (Table S1 and Fig. S3B).

3.6. Ferroptosis increases with age in various organs

We studied all the major organs of rats through the entire life whether ferroptosis is involved in the physiological processes, using HNEJ-1 immunohistochemistry. There was an age-dependent increase in ferroptotic cells in the kidney, spleen, liver, ovary and uterus, which was accompanied by substantial iron accumulation (Figs. 5 and 6). A significant proportional association between iron staining and HNEJ-1 was observed with aging in the kidney, spleen, ovary and uterus, but not in the liver (Fig. S4). In the aged kidney, HNEJ-1 showed cytoplasmic immunostaining in the majority of proximal tubular cells (Fig. 5D). In the aged spleen, liver, ovary and uterus, HNEJ-1 showed immunostaining mainly in macrophages/Kupffer cells, as indicated by CD68 immunostaining on serial sections, whereas there was also positivity in the stroma of ovary and in uterus myometrium as well as parenchymal cells (Fig. 6D). Moreover, increased immunostaining was observed in Purkinje cells and bone marrow in an age-dependent manner (Fig. S5). Elevated expression of ACSL4 was observed in the aged liver, kidney and ovary whereas increased PTGS2 expression was shown in the aged spleen, kidney and ovary (Figs. S6 and S7).

3.7. Ferroptosis in skin senescence model

We extended our study to a skin senescence model, using senescence-accelerated *SAMP8* mice. An increase in the indicators of skin senescence, atrophic epidermal cells with hyalinized collagen (Fig. 7A), was observed in the high fat (HF) diet group as compared to the control (CTRL) group, which was further increased in carbohydrate restricted (CHR) diet group. Immunohistochemical analysis of 8-OHdG revealed that nuclear staining of HF and CHR diet groups is much stronger in epidermal cells than in those of the CTRL group (Fig. 7B). Next, we applied HNEJ-1 on the epidermis, and found that ferroptotic cells were significantly increased in the HF and CHR diet groups in comparison to the CTRL group, which was consistent with senescence (Fig. 7C). Of note, increased expression of PTGS2 but not of ACSL4 was observed in the HF and CHR diet groups in comparison to the CTRL group (Fig. S8).

3.8. Ferroptosis is involved in embryonic erythropoiesis

We then studied the involvement of ferroptosis in different stages of embryonic development of rats, using HNEJ-1. At the stage of E9.5, we observed ferroptosis in extra-embryonic endodermal component of visceral yolk sac (Fig. 8A). As visceral endoderm plays an active role in induction of blood precursors in early mouse embryos [36], we hypothesized that ferroptotic events might be involved in embryo hematopoiesis. Furthermore, we also found ferroptotic process in trophoblast giant cells (TGCs) (Fig. 8B). In addition, high expression of ACSL4 was observed in TGCs at this stage, whereas PTGS2 expression remained low (Fig. S9AB).

At E13.5, nucleated erythrocytes in embryos showed signs of ferroptosis. Of note, not only the level of HNE modification in erythrocytes but also the fraction of HNE-positive erythrocytes subsequently decreased as they enucleated during the process of maturation (E15 and E18) (Fig. 8C). However, ACSL4 and PTGS2 expression was not observed in erythrocytes from E13.5 to E18.5 (Fig. S9C). To further investigate whether ferroptosis is involved in embryonic erythropoiesis, pregnant rats (E13.5) were treated with two ferroptosis inhibitors (Lipro-1 or Fer-1). At E18, the percentage of nucleated erythrocytes in embryos from either Lipro-1 or Fer-1 group were elevated in comparison to those from control groups (Fig. 8D and Fig. S10A). Lamin B, a nuclear marker, of embryonic blood was increased by immunoblot in the Lipro-1 group compared to the control groups, whereas no significance was detected between Fer-1 and the control group (Fig. 8E and Fig. S10B). Increased

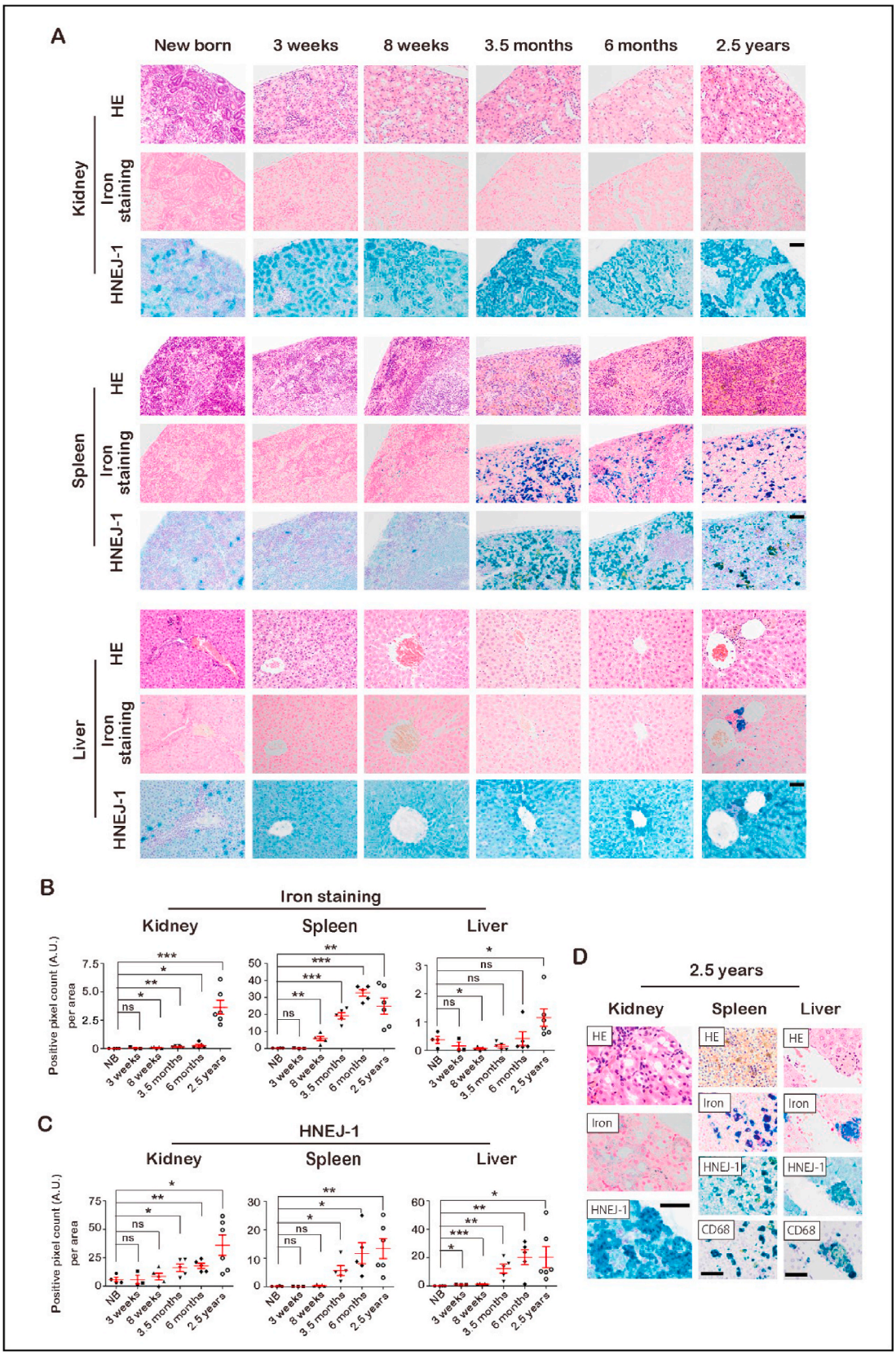

Fig. 5. *HNEJ-1 as a ferroptosis marker for the detection of physiological ferroptosis in kidney, spleen and liver.* **(A)** HE staining, Berlin blue staining and immunostaining with HNEJ-1 for kidney, liver and spleen in different developmental stages of Fischer-344 rats (scale bar = 50 μm). **(B)** Quantification of iron deposits in kidney, liver and spleen in different developmental stages of Fischer-344 rats. **(C)** Quantification of HNE-modified proteins in kidney, liver and spleen in different developmental stages of Fischer-344 rats. **(D)** Serial immunostaining of Berlin blue staining, HNEJ-1 and CD68 in the aged kidney, liver and spleen (scale bar = 50 μm). Representative data are shown based on 3 independent experiments and the analysis is shown as means ± SEM (n = 3–6); *P < 0.05, **P < 0.01, ***P < 0.001 *vs* new born (NB). (For interpretation of the references to color in this figure legend, the reader is referred to the Web version of this article.)

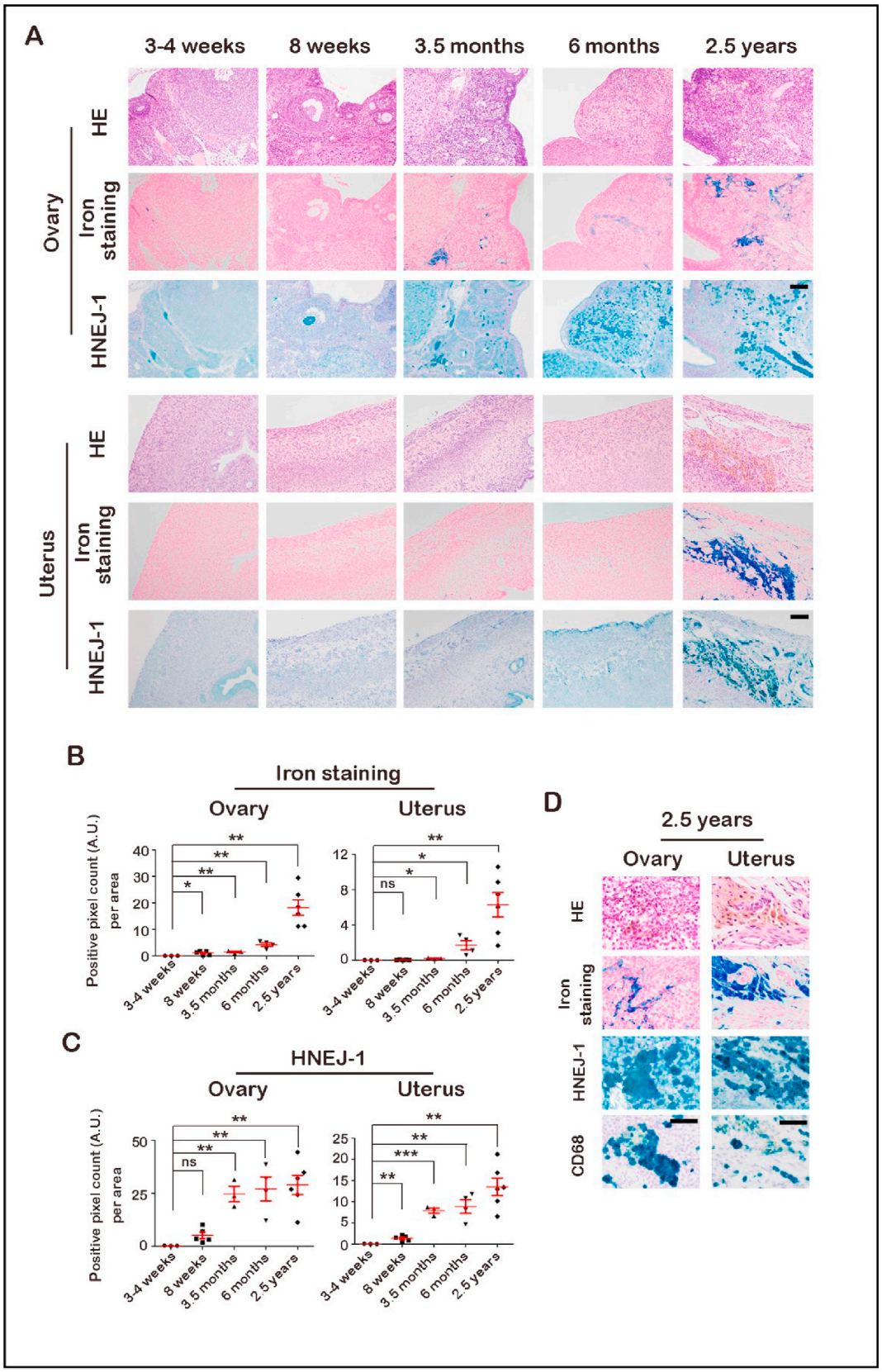

Fig. 6. *HNEJ-1 as a ferroptosis marker for the detection of physiological ferroptosis in ovary and uterus.* (A) HE staining, Berlin blue staining and immunostaining with HNEJ-1 for ovary and uterus in different developmental stages of Fischer-344 rats (scale bar = 50 μm). **(B)** Quantification of iron deposits in ovary and uterus in different developmental stages of Fischer-344 rats. **(C)** Quantification of HNE-modified proteins in ovary and uterus in different developmental stages of Fischer-344 rats. **(D)** Serial immunostaining of Berlin blue staining, HNEJ-1 and CD68 in the aged ovary and uterus (scale bar = 50 μm). Representative data are shown based on 3 independent experiments and the analysis is shown as means ± SEM (n = 3–6); *P < 0.05, **P < 0.01, ***P < 0.001 *vs* 3-4 weeks. (For interpretation of the references to color in this figure legend, the reader is referred to the Web version of this article.)

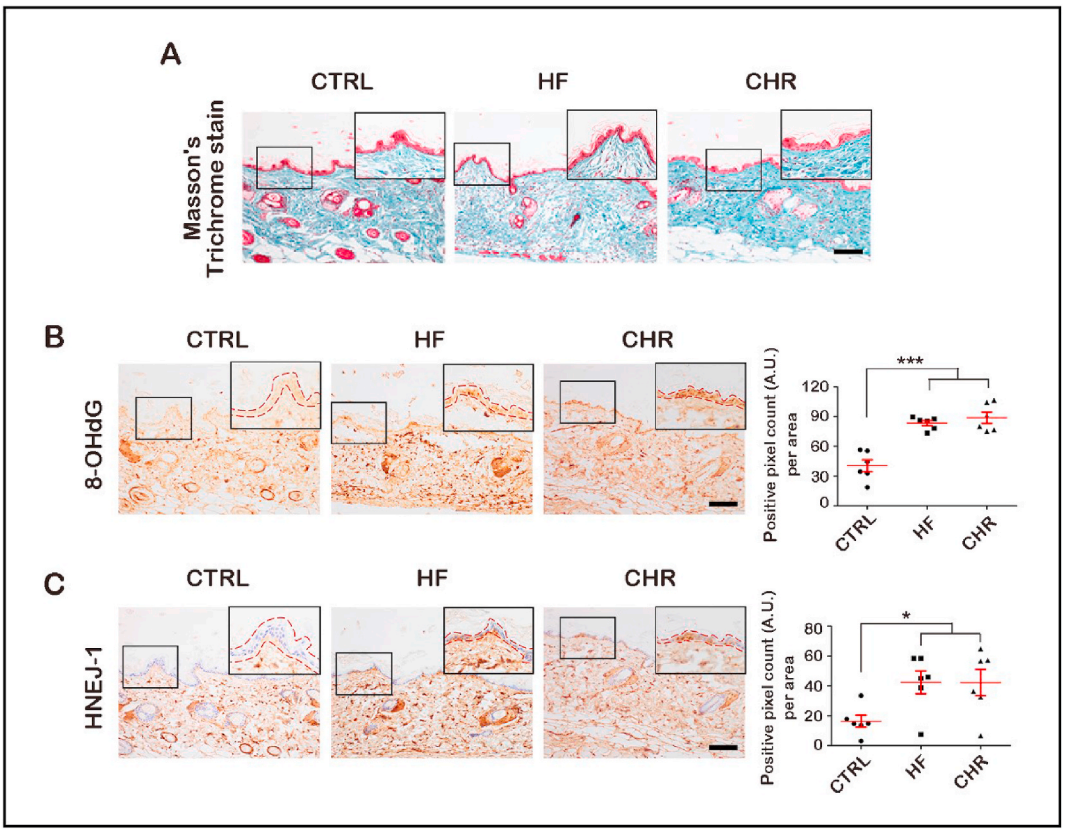

Fig. 7. *HNE modification in skin senescence.* (A) Masson's trichrome staining of CTRL group (*SAMP8* mice; normal diet); HF group (*SAMP8* mice; high-fat diet), and CHR group (*SAMP8* mice; carbohydrate-restricted diet; scale bar = 100 μm). **(B)** Immunostaining and quantification with 8-OHdG for CTRL group, HF group and CHR group (scale bar = 100 μm). **(C)** Immunostaining and quantification with HNEJ-1 for CTRL group, HF group and CHR group (scale bar = 100 μm). Representative data are shown from 3 independent experiments and the analysis is shown as means ± SEM (n = 6); *P < 0.05, **P < 0.01, ***P < 0.001 *vs* CTRL group. Refer to text for details.

TfR1 expression is responsible for the iron uptake during erythropoiesis [37]. Decreased level of TfR1 was observed in Fer-1 group in comparison to the control group, whereas no significance was observed between Lipro-1 and the control group (Fig. 8E and Fig. S10B). Taken together, the results indicate the involvement of ferroptotic signaling in embryonic hematopoiesis, especially erythropoiesis.

4. Discussion

Based on the results presented here, we propose that HNEJ-1 mouse monoclonal antibody, which recognizes HNE-derived Michael adducts equally on His, Lys and Cys residues [27,28], is appropriate for monitoring ferroptotic events. Using this non-selective screening through the entire life of rats, we discovered for the first time that ferroptosis is involved in embryonic erythropoiesis and in aging processes of various organs. This suggests that ferroptosis can have a physiological meaning. We believe that ferroptosis-sensitized cells may not necessarily execute cell death in some cases as in autophagy [38] but can be a driving force for the following metamorphosis or selective process.

In the present study, ferroptosis was observed in the extraembryonic endodermal component of visceral yolk sac (E9.5). The visceral endoderm overlying the extraembryonic mesoderm reportedly influences the differentiation and development of blood islands and vessels [36]. Pre-streak embryonic ectoderm stripped of visceral endoderm is unable to give rise to primitive erythroblasts or express embryonic globin genes in culture, whereas recombination of embryonic ectoderm explants with visceral endoderm allows primitive hematopoiesis to be recovered [39]. Moreover, ferroptotic cell death was observed in trophoblast giant cells (TGCs), which produce a broad range of hormones that regulate several maternal adaptations to pregnancy [40]. Prolactin-like protein (PLP) family members, exclusively expressed in TGCs in particular, were secreted for the regulation of hematopoiesis [41]. PLP-protein E has been shown to stimulate human and mouse erythroid progenitor cell proliferation and differentiation through activation of the JAK/STAT pathway [42]. Our findings suggest the possible involvement of ferroptosis in the induction of hematopoiesis during the embryonic development in rats. On the other hand, a detrimental role of accumulated HNE-protein adducts in placenta has been reported to affect the growth of the fetus [43], indicating that a precise regulation of HNE-modification/ferroptosis determines the threshold between proper embryonic development and pathological processes.

Although erythrocytes are characterized by high iron requirements to sustain hemoglobin synthesis [37], the role of ferroptosis in erythropoiesis has not been clearly shown. In healthy individuals, erythroid cells contain a pool of antioxidant enzymes, including membrane oxidoreductases, superoxide dismutases and catalase, antioxidant scavengers, such as glutaredoxins, thioredoxins and peroxiredoxins, to control cellular redox balance and protect the cells against pro-oxidant damage [44]. Knockout of GPX4, a negative regulator of ferroptosis, was lethal at early embryonic stage due to failure to form well-organized embryonic structures [44]. In a study using mice with hematopoietic cell-specific GPX4-deficiency, ineffective erythropoiesis was observed and the maturation of reticulocytes to erythrocytes was defective [45]. On the one hand, GPX4 was shown to suppress necroptosis instead of ferroptosis in mouse erythroid precursors [46]. On the other hand, a recent study revealed the role of GPX4 in the human erythroblast enucleation in a ferroptosis- and necroptosis-independent manner [47], which indicated its intricate role as a ferroptosis regulator in the process of

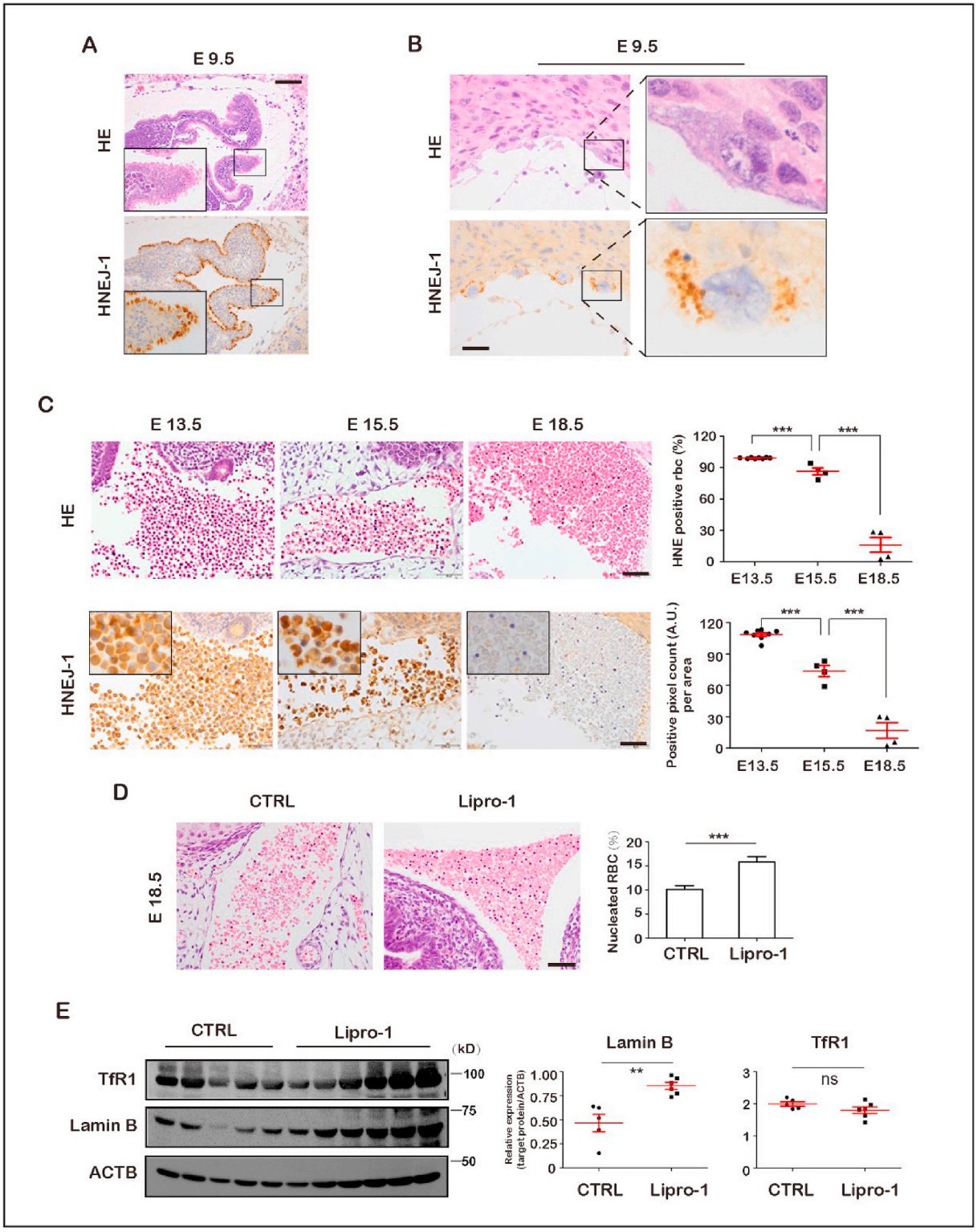

Fig. 8. *Ferroptotic events are involved in embryonic hematopoiesis.* (A) HNE modification in extra-embryonic endodermal component of visceral yolk sac at the stage of E9.5 (n = 5; scale bar = 100 μm). **(B)** HNE modification in trophoblast giant cells at the stage of E9.5 (n = 5; scale bar = 50 μm). **(C)** Rat embryos (Fischer-344) in different stages (E13.5, E15.5 and E18.5) were collected and fixed with 10% neutral buffered formalin for HE staining and immunostaining with HNEJ-1. HNE modification of nucleated red blood cells (RBC) was quantified as percentage of positive cells and positive pixel count (A.U.) per cell (n = 4–8; scale bar = 50 μm). **(D)** Percentage of RBC in embryos from control group and Lipro-1 group (n = 3) were calculated as number of nucleated RBC/total number of RBC from at least 4 embryos per pregnant rat (scale bar = 50 μm). **(E)** Immunoblot analysis of Lamin B and Transferrin receptor 1 (TfR1) in embryos from control group and Lipro-1 group. Representative data are shown based on 3 independent experiments and the analysis is shown as means ± SEM, ***P < 0.001 *vs* E13 or CTRL unless indicated by bar. (For interpretation of the references to color in this figure legend, the reader is referred to the Web version of this article.)

erythropoiesis.

Indeed, 15-lipoxygenase (LOX), which directly oxidizes phosphatidylethanolamines to generate lipid hydroperoxides, is highly expressed in reticulocytes [48,49]. Whereas an early work found that erythrocyte and reticulocyte count were normal in 12/15-LOX knockout mice [50], a recent study revealed that the blood of *15-LOX*$^{-/-}$ mice involved an increased proportion of structurally modified erythrocytes, although the structural and functional differences between *wild-type* and *15-LOX*$^{-/-}$ erythrocytes are not very profound [51]. Erythropoietin reportedly affects enucleation negatively in association with cellular ROS [52]. Conversely, a high dose of ROS inhibitor also deteriorates normal erythropoiesis, indicating that a low level of oxidative stress plays a role in the terminal erythropoiesis [52]. Our results revealed a high level of HNE modification in nucleated erythrocytes. Notably, not only the level of HNE modification in erythrocytes but also the percentage of HNE-positive erythrocytes subsequently decreased according with enucleation during the maturation process. Ferroptosis inhibitors delayed embryonic erythropoiesis, suggesting a positive role of lipid peroxidation during the maturation of erythrocytes. ACSL4 and PTGS2 were almost undetectable in embryonic erythrocytes, indicating that high iron requirement is a major contributing factor to the ferroptotic pathway in embryonic erythrocyte maturation. Our hypothesis is supported by the finding that suppression of ACSL4 expression only decreased malondialdehyde production but not ferrous iron accumulation in HepG2 and HL60 cells following erastin treatment [17].

One major outstanding question is whether ferroptosis is adaptive or indicative of biochemical failure in cells [2]. Here, we observed an age-dependent increase in ferroptosis in the kidney, spleen, liver, ovary and uterus, which was accompanied by iron accumulation in Fischer-344 rats detected by HNEJ-1. As the majority of the iron required to support heme biosynthesis in erythroblasts originates from senescent RBC engulfed by erythrophagocytic macrophages in the red pulp of the spleen, the bone marrow and to some extent in the liver [53], our results indicated the association of ferroptosis and aging, with the participation of macrophages in spleen, liver, ovary, uterus and bone marrow. Furthermore, ferroptosis was significantly higher in the epidermis of *SAMP8* mice, fed with high-fat or carbohydrate-restricted diets, suggesting that they are aggravating factors of skin aging. Sublethal concentration of HNE skin fibroblasts has an impact on the proliferative capacity of fibroblasts during *in vitro* aging [54]. HNE modification to serum proteins was significantly increased by 2–3 fold in old Fischer-344 rats [55]. HNE indeed increased during aging in the blood and plasma of 194 healthy humans, ranging from 18 to 84 years [56]. Because the principal role of red pulp macrophages in spleen and Kupffer cells in liver is to actively phagocytose senescent erythrocytes [53], macrophage ferroptosis with significant iron accumulation, as seen in asbestos pathology [57], may regulate and can be a marker of aging. These results stress the involvement of ferroptosis in physiological senescence. Our observation is supported by a mouse model of red blood cell (RBC) transfusion and clearance, where transfusions of old RBCs led to increased erythrophagocytosis by splenic red pulp macrophages, inducing ferroptosis in macrophages [58].

We also obtained fundamental data for further study of ferroptosis by comprehensively identifying HNE-modified proteins with HNEJ-1 in the rat kidney. Proteins involved in maintaining mitochondrial function are likely to be the main targets of HNE modification in the Fe-NTA-induced acute renal injury model. Aldehyde dehydrogenase, involved in metabolizing HNE and other toxic aldehydes [59], appears among the main targets of HNE modification, which indicated that activities of enzymes involved in the clearance of HNE might be inhibited when ferroptosis started. Among the top 20 proteins, 6 histone proteins were identified (Table S1). Histone release from dying tubular cells has been implicated in acute tubular injury [60]. Histones have been recognized as a target for HNE modification because of their abundant lysine residues [61]. Finally, we noticed that various proteins associated with iron metabolism, such as ferritin and hemopexin, are impaired in addition to antioxidative enzymes, including xanthine dehydrogenase. Further studies are in progress to understand ferroptosis.

In conclusion, the mouse monoclonal antibody HNEJ-1 is useful for screening ferroptotic events in formalin-fixed paraffin-embedded specimens in addition to other reported ferroptosis markers, such as ACSL4 and PTGS2. We summarized the characteristics of each antibody in Table S2. We discovered ferroptosis in embryonic hematopoiesis/erythropoiesis and aging, using this method. Thus, we propose that physiological ferroptosis exists, which may work for the subsequent metamorphosis or selective process in addition to aging.

Declaration of competing interest

The authors except MC declare no conflict of interest. MC holds patents for the compound class of liproxstatins and is a cofounder and shareholder of ROSCUE Therapeutics GmbH.

Acknowledgements

This work was supported, in part, by JST CREST (Grant Number JPMJCR19H4) and JSPS Kakenhi (Grant Number JP19H05462 and JP20H05502). Mass spectrometric analyses were supported by Kentaro Taki, Division of Medical Research Engineering, Nagoya University Graduate School of Medicine. We thank Nobuaki Misawa (Department Pathology and Biological Responses, Nagoya University Graduate School of Medicine) for excellent technical assistance. Work in the Conrad laboratory is supported by funding from the Deutsche Forschungsgemeinschaft (DFG) CO 291/7-1, CO 291/9-1 and CO 291/10-1, the Ministry of Science and Higher Education of the Russian Federation (075-15-2019-1933), and the European Research Council (ERC) under the European Union's Horizon 2020 research and innovation program (Grant Agreement No. GA 884754).

Appendix A. Supplementary data

Supplementary data to this article can be found online at https://doi.org/10.1016/j.redox.2021.102175.

References

[1] S.J. Dixon, K.M. Lemberg, M.R. Lamprecht, R. Skouta, E.M. Zaitsev, C.E. Gleason, D.N. Patel, A.J. Bauer, A.M. Cantley, W.S. Yang, Ferroptosis: an iron-dependent form of nonapoptotic cell death, Cell 149 (5) (2012) 1060–1072.

[2] B.R. Stockwell, J.P. Friedmann Angeli, H. Bayir, A.I. Bush, M. Conrad, S.J. Dixon, S. Fulda, S. Gascon, S.K. Hatzios, V.E. Kagan, K. Noel, X. Jiang, A. Linkermann, M. E. Murphy, M. Overholtzer, A. Oyagi, G.C. Pagnussat, J. Park, Q. Ran, C. S. Rosenfeld, K. Salnikow, D. Tang, F.M. Torti, S.V. Torti, S. Toyokuni, K. A. Woerpel, D.D. Zhang, Ferroptosis: a regulated cell death nexus linking metabolism, Redox Biology, and Disease, Cell 171 (2) (2017) 273–285.

[3] S. Toyokuni, I. Yanatori, Y. Kong, H. Zheng, Y. Motooka, L. Jiang, Ferroptosis at the crossroads of infection, aging and cancer, Cancer Sci. 111 (2020) 2665–2671.

[4] S. Toyokuni, F. Ito, K. Yamashita, Y. Okazaki, S. Akatsuka, Iron and thiol redox signaling in cancer: an exquisite balance to escape ferroptosis, Free Radic. Biol. Med. 108 (2017) 610–626.

[5] S.J. Guiney, P.A. Adlard, A.I. Bush, D.I. Finkelstein, S. Ayton, Ferroptosis and cell death mechanisms in Parkinson's disease, Neurochem. Int. 104 (2017) 34–48.

[6] A. Stamenkovic, K.A. O'Hara, D.C. Nelson, T.G. Maddaford, A.L. Edel, G. Maddaford, E. Dibrov, M. Aghanoori, L.A. Kirshenbaum, P. Fernyhough, M. Aliani, G.N. Pierce, A. Ravandi, Oxidized phosphatidylcholines trigger ferroptosis in cardiomyocytes during ischemia-reperfusion injury, Am. J. Physiol. Heart Circ. Physiol. 320 (3) (2021) H1170–H1184.

[7] R. Skouta, S.J. Dixon, J. Wang, D.E. Dunn, M. Orman, K. Shimada, P.A. Rosenberg, D.C. Lo, J.M. Weinberg, A. Linkermann, B.R. Stockwell, Ferrostatins inhibit oxidative lipid damage and cell death in diverse disease models, J. Am. Chem. Soc. 136 (12) (2014) 4551–4556.

[8] L. Chen, W.S. Hambright, R. Na, Q. Ran, Ablation of the ferroptosis inhibitor glutathione peroxidase 4 in neurons results in rapid motor neuron degeneration and paralysis, J. Biol. Chem. 290 (47) (2015) 28097–28106.

[9] B. Do Van, F. Gouel, A. Jonneaux, K. Timmerman, P. Gele, M. Petrault, M. Bastide, C. Laloux, C. Moreau, R. Bordet, D. Devos, J.C. Devedjian, Ferroptosis, a newly characterized form of cell death in Parkinson's disease that is regulated by PKC, Neurobiol. Dis. 94 (2016) 169–178.

[10] W.S. Hambright, R.S. Fonseca, L. Chen, R. Na, Q. Ran, Ablation of ferroptosis regulator glutathione peroxidase 4 in forebrain neurons promotes cognitive impairment and neurodegeneration, Redox Biol. 12 (2017) 8–17.

[11] S. Toyokuni, Role of iron in carcinogenesis: cancer as a ferrotoxic disease, Cancer Sci. 100 (1) (2009) 9–16.

[12] S. Toyokuni, Y. Kong, Z. Cheng, K. Sato, S. Hayashi, F. Ito, L. Jiang, I. Yanatori, Y. Okazaki, S. Akatsuka, Carcinogenesis as side effects of iron and oxygen utilization: from the unveiled truth toward ultimate bioengineering, Cancers (Basel) 12 (11) (2020) 3320.

[13] M.J. Hangauer, V.S. Viswanathan, M.J. Ryan, D. Bole, J.K. Eaton, A. Matov, J. Galeas, H.D. Dhruv, M.E. Berens, S.L. Schreiber, F. McCormick, M.T. McManus, Drug-tolerant persister cancer cells are vulnerable to GPX4 inhibition, Nature 551 (7679) (2017) 247–250.

[14] V.S. Viswanathan, M.J. Ryan, H.D. Dhruv, S. Gill, O.M. Eichhoff, B. Seashore-Ludlow, S.D. Kaffenberger, J.K. Eaton, K. Shimada, A.J. Aguirre, S.R. Viswanathan, S. Chattopadhyay, P. Tamayo, W.S. Yang, M.G. Rees, S. Chen, Z.V. Boskovic, S. Javaid, C. Huang, X. Wu, Y.Y. Tseng, E.M. Roider, D. Gao, J.M. Cleary, B. M. Wolpin, J.P. Mesirov, D.A. Haber, J.A. Engelman, J.S. Boehm, J.D. Kotz, C. S. Hon, Y. Chen, W.C. Hahn, M.P. Levesque, J.G. Doench, M.E. Berens, A.F. Shamji, P.A. Clemons, B.R. Stockwell, S.L. Schreiber, Dependency of a therapy-resistant state of cancer cells on a lipid peroxidase pathway, Nature 547 (7664) (2017) 453–457.

[15] L. Jiang, H. Zheng, Q. Lyu, S. Hayashi, K. Sato, Y. Sekido, K. Nakamura, H. Tanaka, K. Ishikawa, H. Kajiyama, M. Mizuno, M. Hori, S. Toyokuni, Lysosomal nitric oxide determines transition from autophagy to ferroptosis after exposure to plasma-activated Ringer's lactate, Redox Biol. 43 (2021) 101989.

[16] Y. Li, D. Feng, Z. Wang, Y. Zhao, R. Sun, D. Tian, D. Liu, F. Zhang, S. Ning, J. Yao, X. Tian, Ischemia-induced ACSL4 activation contributes to ferroptosis-mediated tissue injury in intestinal ischemia/reperfusion, Cell Death Differ. 26 (11) (2019) 2284–2299.

[17] H. Yuan, X. Li, X. Zhang, R. Kang, D. Tang, Identification of ACSL4 as a biomarker and contributor of ferroptosis, Biochem. Biophys. Res. Commun. 478 (3) (2016) 1338–1343.

[18] S.J. Dixon, G.E. Winter, L.S. Musavi, E.D. Lee, B. Snijder, M. Rebsamen, G. Superti-Furga, B.R. Stockwell, Human haploid cell genetics reveals roles for lipid metabolism genes in nonapoptotic cell death, ACS Chem. Biol. 10 (7) (2015) 1604–1609.

[19] W.S. Yang, R. SriRamaratnam, M.E. Welsch, K. Shimada, R. Skouta, V. S. Viswanathan, J.H. Cheah, P.A. Clemons, A.F. Shamji, C.B. Clish, L.M. Brown, A. W. Girotti, V.W. Cornish, S.L. Schreiber, B.R. Stockwell, Regulation of ferroptotic cancer cell death by GPX4, Cell 156 (1–2) (2014) 317–331.

[20] Y. Ebina, S. Okada, S. Hamazaki, F. Ogino, J.L. Li, O. Midorikawa, Nephrotoxicity and renal cell carcinoma after use of iron- and aluminum- nitrilotriacetate complexes in rats, J. Natl. Cancer Inst. 76 (1986) 107–113.

[21] Y. Nishiyama, H. Suwa, K. Okamoto, M. Fukumoto, H. Hiai, S. Toyokuni, Low incidence of point mutations in *H-, K-* and *N-ras* oncogenes and *p53* tumor suppressor gene in renal cell carcinoma and peritoneal mesothelioma of Wistar rats induced by ferric nitrilotriacetate, Jpn. J. Cancer Res. 86 (1995) 1150–1158.

[22] S. Akatsuka, Y. Yamashita, H. Ohara, Y.T. Liu, M. Izumiya, K. Abe, M. Ochiai, L. Jiang, H. Nagai, Y. Okazaki, H. Murakami, Y. Sekido, E. Arai, Y. Kanai, O. Hino, T. Takahashi, H. Nakagama, S. Toyokuni, Fenton reaction induced cancer in wild type rats recapitulates genomic alterations observed in human cancer, PLoS One 7 (8) (2012), e43403.

[23] S. Toyokuni, The origin and future of oxidative stress pathology: from the recognition of carcinogenesis as an iron addiction with ferroptosisresistance to non-thermal plasma therapy, Pathol. Int. 66 (2016) 245–259.

[24] S. Toyokuni, Iron-induced carcinogenesis: the role of redox regulation, Free Radic. Biol. Med. 20 (1996) 553–566.

[25] S. Toyokuni, K. Uchida, K. Okamoto, Y. Hattori-Nakakuki, H. Hiai, E.R. Stadtman, Formation of 4-hydroxy-2-nonenal-modified proteins in the renal proximal tubules of rats treated with a renal carcinogen, ferric nitrilotriacetate, Proc. Natl. Acad. Sci. U.S.A. 91 (1994) 2616–2620.

[26] S. Toyokuni, X.P. Luo, T. Tanaka, K. Uchida, H. Hiai, D.C. Lehotay, Induction of a wide range of $C_{2\text{-}12}$ aldehydes and $C_{7\text{-}12}$ acyloins in the kidney of Wistar rats after treatment with a renal carcinogen, ferric nitrilotriacetate, Free Radic. Biol. Med. 22 (1997) 1019–1027.

[27] S. Toyokuni, N. Miyake, H. Hiai, M. Hagiwara, S. Kawakishi, T. Osawa, K. Uchida, The monoclonal antibody specific for the 4-hydroxy-2-nonenal histidine adduct, FEBS Lett. 359 (2–3) (1995) 189–191.

[28] M. Ozeki, A. Miyagawa-Hayashino, S. Akatsuka, T. Shirase, W.H. Lee, K. Uchida, S. Toyokuni, Susceptibility of actin to modification by 4-hydroxy-2-nonenal, J. Chromatogr. B Analyt. Technol. Biomed. Life Sci. 827 (1) (2005) 119–126.

[29] J.P.F. Angeli, M. Schneider, B. Proneth, Y.Y. Tyurina, V.A. Tyurin, V.J. Hammond, N. Herbach, M. Aichler, A. Walch, E. Eggenhofer, Inactivation of the ferroptosis regulator Gpx4 triggers acute renal failure in mice, Nat. Cell Biol. 16 (12) (2014) 1180.

[30] Q.M. Wu, E. Shuang, K. Yamamoto, T. Tsuduki, Carbohydrate-restricted diet promotes skin senescence in senescence-accelerated prone mice, Biogerontology 20 (1) (2019) 71–82.

[31] S. Toyokuni, T. Tanaka, Y. Hattori, Y. Nishiyama, H. Ochi, H. Hiai, K. Uchida, T. Osawa, Quantitative immunohistochemical determination of 8-hydroxy-2'-deoxyguanosine by a monoclonal antibody N45.1: its application to ferric nitrilotriacetate-induced renal carcinogenesis model, Lab. Invest. 76 (1997) 365–374.

[32] S. Li, M. Jiang, L. Wang, S. Yu, Combined chemotherapy with cyclooxygenase-2 (COX-2) inhibitors in treating human cancers: recent advancement, Biomed. Pharmacother. 129 (2020) 110389.

[33] R. Brea, O. Motino, D. Frances, C. Garcia-Monzon, J. Vargas, M. Fernandez-Velasco, L. Bosca, M. Casado, P. Martin-Sanz, N. Agra, PGE2 induces apoptosis of hepatic stellate cells and attenuates liver fibrosis in mice by downregulating miR-23a-5p and miR-28a-5p, Biochim. Biophys. Acta (BBA) - Mol. Basis Dis. 1864 (2) (2018) 325–337.

[34] K. Yamaki, T. Yonezawa, K. Ohuchi, Signal transduction cascade in staurosporine-induced prostaglandin E(2) production by rat peritoneal macrophages, J. Pharmacol. Exp. Therapeut. 293 (1) (2000) 206–213.

[35] K. Uchida, L.I. Szweda, H.Z. Chae, E.R. Stadtman, Immunochemical detection of 4-hydroxynonenal protein adducts in oxidized hepatocytes, Proc. Natl. Acad. Sci. U. S.A. 90 (18) (1993) 8742–8746.

[36] D.M. Boucher, R.A. Pedersen, Induction and differentiation of extra-embryonic mesoderm in the mouse, Reprod. Fertil. Dev. 8 (4) (1996) 765–777.

[37] M.U. Muckenthaler, S. Rivella, M.W. Hentze, B. Galy, A red carpet for iron metabolism, Cell 168 (3) (2017) 344–361.

[38] D.J. Klionsky, A.K. Abdel-Aziz, S. Abdelfatah, M. Abdellatif, A. Abdoli, S. Abel, et al., Guidelines for the use and interpretation of assays for monitoring autophagy, Autophagy 17 (1) (2021) 1–382, 4th edition)(1.

[39] M. Belaoussoff, S.M. Farrington, M.H. Baron, Hematopoietic induction and respecification of A-P identity by visceral endoderm signaling in the mouse embryo, Development 125 (24) (1998) 5009–5018.

[40] D. Hu, J.C. Cross, Development and function of trophoblast giant cells in the rodent placenta, Int. J. Dev. Biol. 54 (2–3) (2010) 341–354.

[41] B.Y. Zhou, X.R. Kong, D.I.H. Linzer, Enhanced recovery from thrombocytopenia and neutropenia in mice constitutively expressing a placental hematopoietic cytokine, Endocrinology 146 (1) (2005) 64–70.

[42] T. Bittorf, R. Jaster, M.J. Soares, J. Seiler, J. Brock, K. Friese, H. Muller, Induction of erythroid proliferation and differentiation by a trophoblast-specific cytokine involves activation of the JAK/STAT pathway, J. Mol. Endocrinol. 25 (2) (2000) 253–262.

[43] S. Gveric-Ahmetasevic, S.B. Sunjic, H. Skala, L. Andrisic, M. Stroser, K. Zarkovic, S. Skrablin, F. Tatzber, A. Cipak, M. Jaganjac, G. Waeg, T. Gveric, N. Zarkovic, Oxidative stress in small-for-gestational age (SGA) term newborns and their mothers, Free Radic. Res. 43 (4) (2009) 376–384.

[44] C. Liao, B.A. Carlson, R.F. Paulson, K.S. Prabhu, The intricate role of selenium and selenoproteins in erythropoiesis, Free Radic. Biol. Med. 127 (2018) 165–171.

[45] S. Altamura, N.M. Vegi, P.S. Hoppe, T. Schroeder, M. Aichler, A. Walch, K. Okreglicka, L. Hultner, M. Schneider, C. Ladinig, C. Kuklik-Roos, J. Mysliwietz, D. Janik, F. Neff, B. Rathkolb, M.H. de Angelis, C. Buske, A.R. da Silva, K. Muedder, M. Conrad, T. Ganz, M. Kopf, M.U. Muckenthaler, G.W. Bornkamm, Glutathione peroxidase 4 and vitamin E control reticulocyte maturation, stress erythropoiesis and iron homeostasis, Haematologica 105 (4) (2020) 937–950.

[46] O. Canli, Y.B. Alankus, S. Grootjans, N. Vegi, L. Hultner, P.S. Hoppe, T. Schroeder, P. Vandenabeele, G.W. Bornkamm, F.R. Greten, Glutathione peroxidase 4 prevents necroptosis in mouse erythroid precursors, Blood 127 (1) (2016) 139–148.

[47] H. Ouled-Haddou, K. Messaoudi, Y. Demont, R.L. Dos Santos, C. Carola, A. Caulier, P. Vong, N. Jankovsky, D. Lebon, A. Willaume, J. Demagny, T. Boyer, J. P. Marolleau, J. Rochette, L. Garcon, A new role of glutathione peroxidase 4 during human erythroblast enucleation, Blood Adv. 4 (22) (2020) 5666–5680.

[48] S.M. Rapoport, T. Schewe, R. Wiesner, W. Halangk, P. Ludwig, M. Janickehohne, C. Tannert, C. Hiebsch, D. Klatt, Lipoxygenase of reticulocytes - purification, characterization and biological dynamics of the lipoxygenase - its identity with the respiratory inhibitors of the reticulocyte, Eur. J. Biochem. 96 (3) (1979) 545–561.

[49] H. Kuhn, A.R. Brash, Occurrence of lipoxygenase products in membranes of rabbit reticulocytes. Evidence for a role of the reticulocyte lipoxygenase in the maturation of red cells, J. Biol. Chem. 265 (3) (1990) 1454–1458.

[50] D. Sun, C.D. Funk, Disruption of 12/15-lipoxygenase expression in peritoneal macrophages. Enhanced utilization of the 5-lipoxygenase pathway and diminished oxidation of low density lipoprotein, J. Biol. Chem. 271 (39) (1996) 24055–24062.

[51] M. Rademacher, H. Kuhn, A. Borchert, Systemic deficiency of mouse arachidonate 15-lipoxygenase induces defective erythropoiesis and transgenic expression of the human enzyme rescues this phenotype, Faseb. J. 34 (11) (2020) 14318–14335.

[52] B. Zhao, Y. Mei, J. Yang, P. Ji, Erythropoietin-regulated oxidative stress negatively affects enucleation during terminal erythropoiesis, Exp. Hematol. 44 (10) (2016) 975–981.

[53] M.D. Knutson, M. Oukka, L.M. Koss, F. Aydemir, M. Wessling-Resnick, Iron release from macrophages after erythrophagocytosis is up-regulated by ferroportin 1 overexpression and down-regulated by hepcidin, Proc. Natl. Acad. Sci. U.S.A. 102 (5) (2005) 1324–1328.

[54] I. Petkovic, N. Bresgen, E. Gilardoni, L. Regazzoni, K. Uchida, G. Aldini, W. Siems, P. Eckl, In vitro aging of human skin fibroblasts: age-dependent changes in 4-hydroxynonenal metabolism, Antioxidants (Basel) 9 (2) (2020) 150.

[55] C.H. Kim, Y. Zou, D.H. Kim, N.D. Kim, B.P. Yu, H.Y. Chung, Proteomic analysis of nitrated and 4-hydroxy-2-nonenal-modified serum proteins during aging, J. Gerontol. A Biol. Sci. Med. Sci. 61 (4) (2006) 332–338.

[56] L. Gil, W. Siems, B. Mazurek, J. Gross, P. Schroeder, P. Voss, T. Grune, Age-associated analysis of oxidative stress parameters in human plasma and erythrocytes, Free Radic. Res. 40 (5) (2006) 495–505.

[57] F. Ito, I. Yanatori, Y. Maeda, K. Nimura, S. Ito, T. Hirayama, H. Nagasawa, N. Kohyama, Y. Okazaki, S. Akatsuka, S. Toyokuni, Asbestos conceives Fe(II)-dependent mutagenic stromal milieu through ceaseless macrophage ferroptosis and beta-catenin induction in mesothelium, Redox Biol. 36 (2020) 101616.

[58] L.A. Youssef, A. Rebbaa, S. Pampou, S.P. Weisberg, B.R. Stockwell, E.A. Hod, S. L. Spitalnik, Increased erythrophagocytosis induces ferroptosis in red pulp macrophages in a mouse model of transfusion, Blood 131 (23) (2018) 2581–2593.
[59] H. Zhang, T.E. Morgan, H.J. Forman, Age-related alteration in HNE elimination enzymes, Arch. Biochem. Biophys. 699 (2021) 108749.
[60] R. Allam, C.R. Scherbaum, M.N. Darisipudi, S.R. Mulay, H. Hagele, J. Lichtnekert, J.H. Hagemann, K.V. Rupanagudi, M. Ryu, C. Schwarzenberger, B. Hohenstein, C. Hugo, B. Uhl, C.A. Reichel, F. Krombach, M. Monestier, H. Liapis, K. Moreth, L. Schaefer, H.J. Anders, Histones from dying renal cells aggravate kidney injury via TLR2 and TLR4, J. Am. Soc. Nephrol. 23 (8) (2012) 1375–1388.
[61] J. Drake, R. Petroze, A. Castegna, Q. Ding, J.N. Keller, W.R. Markesbery, M. A. Lovell, D.A. Butterfield, 4-Hydroxynonenal oxidatively modifies histones: implications for Alzheimer's disease, Neurosci. Lett. 356 (3) (2004) 155–158.